Available online at www.sciencedirect.com

SCIENCE DIRECT®

Journal of Molecular Catalysis A: Chemical 199 (2003) 115–137

JOURNAL OF MOLECULAR CATALYSIS A: CHEMICAL

www.elsevier.com/locate/molcata

Review

Design of molecular-imprinting metal-complex catalysts

Mizuki Tada, Yasuhiro Iwasawa*

Department of Chemistry, Graduate School of Science, The University of Tokyo, Hongo, Bunkyo-ku, Tokyo 113-0033, Japan

Received 1 August 2002; received in revised form 10 September 2002; accepted 10 September 2002

Abstract

This article attempted to review novel metal-complex catalysts prepared by molecular-imprinting methods, presenting our work on recent catalyst design at surfaces. Molecular imprinting is a way to produce cavity with a particular molecule (template) by polymerization of organic and inorganic materials and removal of the template. The cavity with memory of the template provides shape-selective reaction space for the molecule which has similar shape to the template. Recently, the application to metal-complex catalysts has been achieved to exploit unique property different from homogeneous and simple supported metal-complex catalysts. Imprinting metal-complex catalysts prepared by using reaction intermediate or transition state analogues as templates for asymmetric hydride transfer reduction of ketones, aldol condensation, and shape-selective hydrogenation of simple alkenes without any functional groups are focused in the viewpoint of new approaches in design of shape-selective metal-complex catalysts.

Keywords: Molecular imprinting; Template; Catalyst design at surface; Selectivity; Metal complex; Rhodium; Ruthenium; Cobalt; Alkene hydrogenation; Asymmetric synthesis

1. Introduction

Synthesis of new artificial enzymes with high catalytic activity and shape-selectivity is one of the attractive subjects in the fields such as catalytic chemistry, surface organometallic chemistry, material chemistry, surface chemistry, etc. Native enzyme catalysts can recognize particular substrate molecules at active centers which possess reaction spaces with substrate-molecular shapes and spatially organized molecular-recognition sites. To prepare artificial enzymatic systems possessing molecular-recognition ability for particular molecules, molecular-imprinting methods which create template-shape cavity with memory of the template molecule in polymer matrices have been developed [1–9] and established to receptor [10–18], chromatographical separations [19,20], fine chemical sensing [21–24], etc. in the past decade. Especially, design of molecularly imprinted catalytic materials and their application to asymmetric catalyses which require the most severe regulation of catalytic sites are one of most wonderful themes in chemistry. Recently, in addition to imprinted acid–base catalysts, some examples of molecular imprinting of metal complexes have been reported and become currently an up-to-date active field. In this review, we outline new syntheses and performances of molecular-imprinting metal-complex catalysts in which reaction intermediate analogues are used as template molecules.

* Corresponding author. Tel.: +81-3-5841-4363; fax: +81-3-5800-6892.
E-mail address: iwasawa@chem.s.u-tokyo.ac.jp (Y. Iwasawa).

1381-1169/03/$ – see front matter © 2003 Elsevier Science B.V. All rights reserved.
doi:10.1016/S1381-1169(03)00029-3

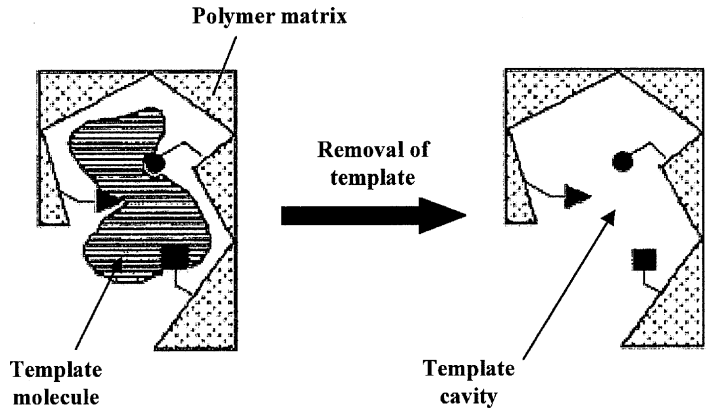

Fig. 1. Principle of molecular-imprinting method to prepare template-shape cavity.

2. Principle and previous attempts of molecular imprinting for catalysts

Principle of creation of cavity with similar shape to template molecule in appropriate matrix by molecular imprinting involves two processes illustrated in Fig. 1. Some organic or inorganic polymer matrices are produced around particular molecules used as template, covering spaces around the templates. Then the template molecules are removed from the polymer matrices, and as the result, template-shape cavities behind the templates are obtained in the matrices, which act as selective recognition spaces for molecules with similar shape to the template.

The first approach to preparation of molecular-imprinting materials traces back to the early stage of 1930s. Poljakow removed water from silica gel in an atmosphere of benzene, toluene or xylene [25]. He found that the pore structure was influenced by the size and shape of the molecules in the gas atmosphere. Silica gel dried in benzene adsorbed faster than toluene or xylene. In 1949, Dickey prepared for the first time imprinted gels from an acidified silica solution in the presence of methyl orange, and after extraction the obtained gels adsorbed methyl orange better than a blank gel [26,27]. After 1950s, such imprinted materials have been produced and applied to receptor and binding assay [10–18], chromatographic separation [19,20] and chemical sensing [21–24], in which adsorption was simply regulated. However, application of the mimic materials to catalytic reactions has been still hard, because catalysis is a dynamic process involving rearrangement of chemical bonds in the substrate molecules. Nevertheless, artificial enzymatic materials synthesized by molecular-imprinting techniques using a variety of template molecules provide promising molecular-recognition catalysis with 100% selectivity for a variety of catalytic reactions where natural enzymes cannot be employed.

In 1980s and the first-half of 1990s, simply modified materials such as SiO_2 gels doped with Al^{3+} as Lewis acid sites to which template molecules were assumed to coordinate, were reported to behave as catalysts for transacylation and 2,4-dinitrophenolysis [28,29]. Recently, more complicated modifications than control of only pore size were performed to synthesize molecular-imprinting catalysts. Organic functional groups inside polymer matrices which had been spatially arranged to be bound to a template molecule brought sophisticated functionality of recognition sites like amino and hydroxyl groups [30–35]. These functional groups act as not only chemical binding sites on the wall of cavities, but also base catalytic sites for various hydrolysis reactions. On the other hand, an imprinted SiO_2 bulk with amino groups on cavity wall acted as an effective catalyst for Knoevenagel condensation reaction [36]. Such inorganic oxide matrices may be more suitable for various catalytic reactions, especially under severe reaction conditions like high temperature and pressure in various solvents. The typical previous reports of molecular imprinting for acid–base catalysts are summarized in Table 1.

Because of difficulty of imprinting at molecular level, most of the studies on molecular-imprinting

Table 1
Examples of imprinted catalysts without metal complexes

Catalytic reaction	Remark	Reference
Butanolysis of benzoic anhydride	"Footprint" catalyst of Al–Si hybrid gels	[37]
Hydrolysis of acetate	Imprinting of transition state analogue by vinylimidasole	[38]
2,4-Dinitrophenolysis	"Footprint" catalyst of Al–Si hybrid gels	[28]
Transacylation	"Footprint" catalyst of Al–Si hybrid gels	[29]
Transesterification	Imprinting of transition state analogue in SiO_2 bulk	[39]
Dehydrofluorination	Cavity with amino binding sites in acrylate polymer matrix	[30]
Hydrolysis of ester	Imprinting of transition state analogue by acrylate polymer	[32]
Hydrolysis of amide	Imprinting of transition state analogue on SiO_2 surface	[40]
Hydrolysis of ester	Binding sites on wall of template cavity in acrylate polymer	[35]
Knoevenagel condensation	Imprinted bulk SiO_2 with binding sites inside template cavity	[36]
Hydrolysis of carbonate and carbamate	Imprinting of transition state analogue by acrylate polymer	[34]
Alkane combustion	Imprinting of organic molecule on SnO_2 surface	[41]
Hydrolysis of ester	Imprinting of transition state analogue on Al_2O_3 surface	[42]

Table 2
Reported molecular-imprinting metal-complex catalysts

Catalytic reaction	Metal	Remark	Reference
Aldol condensation	Co	Bulk imprinting of diketone mimicking a reaction intermediate	[43]
Hydride transfer reduction of ketones	Rh	Bulk polymer imprinting of a reaction intermediate	[44]
Diels–Alder reaction	Ti	Ti complex linked by polymerizable ligands in styrene polymer	[45]
Transfer hydrogenation of ketones	Ru	Bulk imprinting of phosphinate analog of an intermediate	[46]
Transfer hydrogenation of ketones	Rh	Bulk imprinting of phosphinate analog of an intermediate	[47]
Cross-coupling reaction	Pd	Attaching in styrene–divinylbenzene copolymer matrix	[48]
Hydrogenation of alkenes	Rh	Surface imprinting of $P(OCH_3)_3$ ligand of attached Rh monomer	[49]
Hydrogenation of alkenes	Rh	Surface imprinting of $P(OCH_3)_3$ ligand of attached Rh dimer	[50,51]

catalysts have been devoted to acid–base catalysts though many important catalytic reactions have been performed by use of metal and metal complexes. Some trials to imprint metal complexes have been reported, which are summarized in Table 2. In most cases of molecular imprinting for metal complexes, ligands of the complexes were used as template molecules, which aims to create cavity near the metal site as shown in Fig. 2. Molecular imprinting of metal complex enables to realize several features to note: (1) attaching of metal complex to solid material; (2) surrounding of the metal complex by polymer matrix; (3)

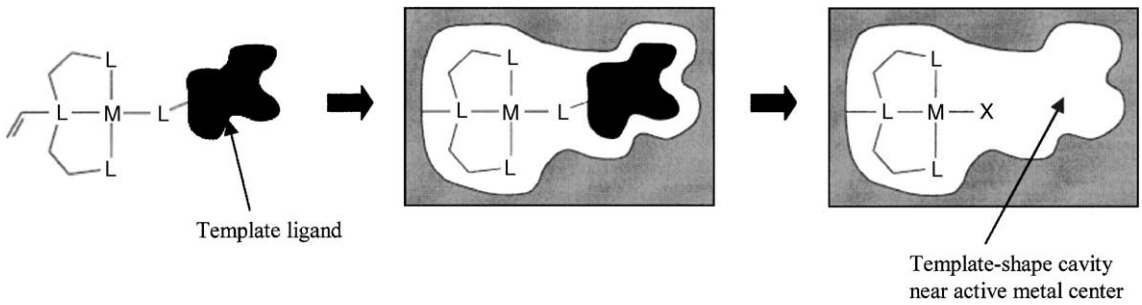

Fig. 2. A schematic representation of molecular imprinting of metal-complex catalyst. Ligand coordinated to metal center is regarded as template molecule. After removal of the template ligand, template-shape cavity is obtained near the metal center.

formation of new active structure in the matrix; and (4) production of shape-selective space near the metal site. To use these features, metal complexes imprinted by polymers have been applied for molecular recognition [52,53], reactive complex stabilization [54,55], ligand exchange reaction [56], and catalyses [43–51]. Particularly, molecular-imprinting metal-complex catalysts can exhibit unique properties compared with homogeneous and simple supported metal complexes, which is most interesting subject at present.

To realize shape-selectivity corresponding to particular molecule at imprinted metal site, it is necessary to use appropriate template ligand, particularly, similar to reaction intermediate or transition state in order to prepare enzyme-mimic catalytic systems. However, template ligands used in most studies were different sizes and shapes without any relation to the reactants [45,48] and there are few reports performed by using suitable templates [43,44,46,47,49–51]. Five imprinted metal-complex catalysts are described in following chapters.

3. Molecular imprinting of metal-complexes in bulk polymers

Metal complex with reaction cavity of the same shape as the transition state of rate-determining step for a catalytic reaction is most appropriate for catalysts, but it is hard to determine their accurate structures. Reaction intermediates before and after the rate-determining step are considered to have similar shapes to the transition state and they are generally used as templates for molecular imprinting [43,44,46,47,49–51]. The imprinting is often performed by polymerization of organic monomers such as ethylene glycol dimethacrylate (EGDMA) or styrene–divinylbenzene copolymer (DVB) and the imprinted metal complexes are located inside bulk polymer matrices [43–48].

The first attempt to imprint metal complex of reaction intermediate was a cobalt catalyst which mimicked a class II aldolase for aldol condensation by Matsui et al. [43]. An aldolase-mimicking imprinted polymer was prepared by the molecular imprinting of a cobalt complex coordinated with dibenzoylmethane. The dibenzoylmethane ligand is regarded as a reactive intermediate analogue of aldol condensation of acetophenone and benzaldehyde. The Co complex coordinated with two vinyl pyridine ligands was copolymerized in styrene and divinylbenzene, which was grafted by the vinyl pyridine linked to the copolymer. Finally, they prepared imprinted polymers possessing cavity of similar shape to the reaction intermediate by removal of the Co complex coordinated with dibenzoylmethane as shown in Fig. 3. Vinyl pyridine ligands remained on the wall of cavity inside the produced polymer matrix disposing to fit the intermediate Co complex. The polymerized monomers were expected to interact with the template dibenzoylmethane through π–π stacking and van del Waals interactions to aid in defining the recognition site topography in the resultant polymer. Reaction rate on the imprinted catalyst increased eight times higher than that of homogenous solution reaction as shown in Fig. 4. In reactions of other ketones substituted for the acetophenone, adamantyl methyl ketone and 9-acetylanthracene on the imprinted polymer, degrees of enhancement of the reaction rates were lower than that of acetophenone, indicating selectivity for the acetophenone molecule. Furthermore, the imprinted catalyst was able to withstand vigorous reaction conditions, DMF and 373 K for several weeks, although natural enzymes are not durable under the severe condition. This is the first attempt to carry out carbon–carbon bond formation using the molecular-imprinting technique.

The molecular-imprinting method is applicable to enantioselective materials as a new tool to asymmetric syntheses. The first trial to use a chiral ligand of metal complex as template was performed by Locatelli et al. in 1998 [44]. A polymerized rhodium complex catalyst was prepared by molecular-imprinting method using a chiral template ligand and catalytic behaviors for asymmetric hydride transfer reduction of ketones were studied. Synthesis procedure of the imprinted Rh polymer is illustrated in Fig. 5. Two chiral diamines ((1*S*,2*S*)-*N*,*N*′-dimethyl-1,2-diphenylethane diamine) were coordinated to $[Rh(C_8H_{12})Cl]_2$ and then optically pure 1-(*S*)-phenylethoxide or 1-(*R*)-phenylethoxide (sodium 1-phenylethanolate) used as template was attached to the Rh complex. Isocyanate (ONC-R-CNO) was polymerized with the obtained Rh complex coordinated with the template ligand to connect the bidentate–diamine ligand to form polymer backbone. Resulting polyurea-containing Rh complex was reacted with isopropanol to extract the template by

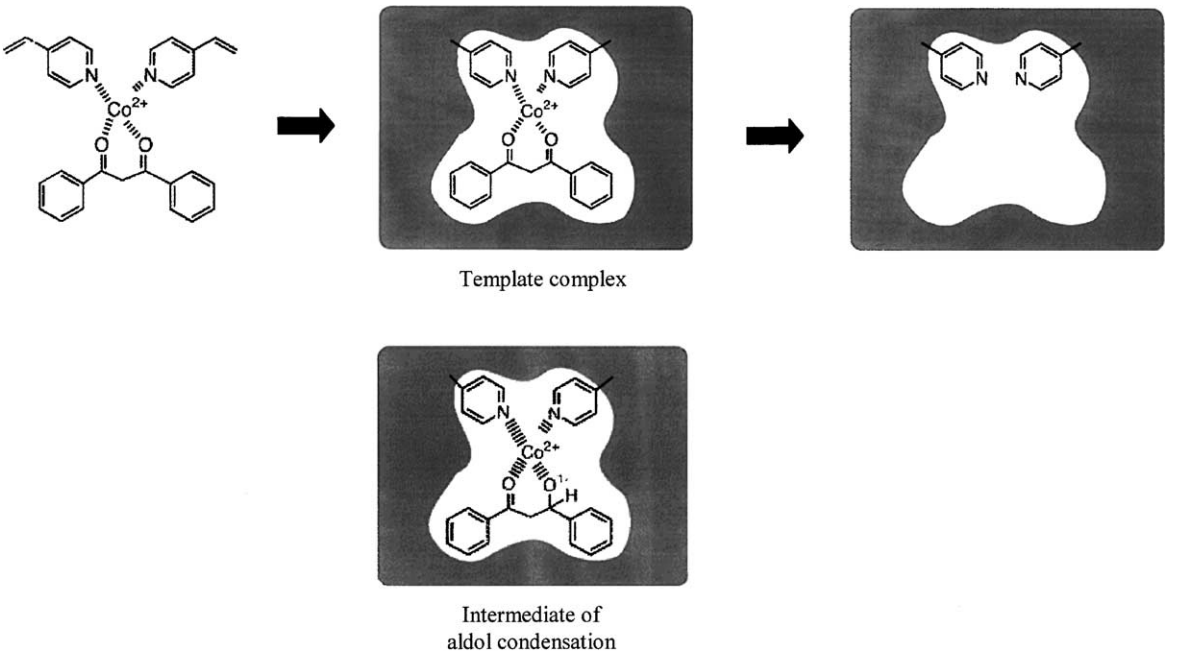

Fig. 3. Synthesis procedure of imprinted cobalt polymer catalyst for aldol condensation of acetophenone and benzaldehyde.

hydride transfer reduction. The template ligand is regarded to possess the same shape as a half-hydrogenated state of acetophenone that is an intermediate of the hydride transfer reduction. Non-imprinted polymer was also prepared by use of chloro ligand instead of the chiral ethoxide template as reference. The reactions were carried out on three catalysts, homogenous Rh complex coordinated with the diamine ligands, the Rh complex supported to polyurea (non-imprinted polymer), and the imprinted polymer prepared in the presence of the chiral template, and they examined the influence to conversion and enantio excess by the

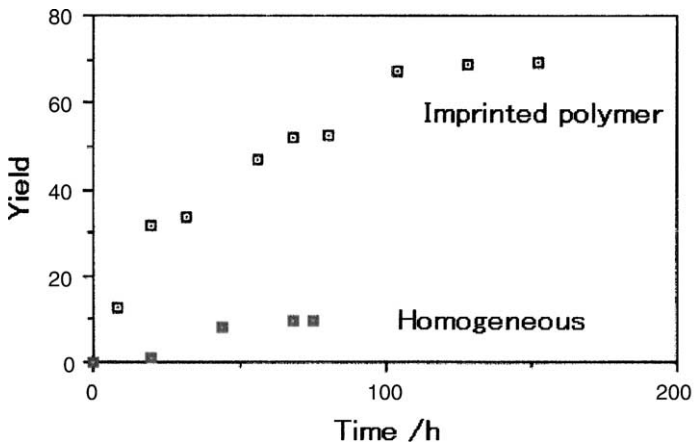

Fig. 4. Reaction rates of aldol condensation of acetophenone and benzaldehyde on the imprinted cobalt catalyst and homogeneous cobalt catalyst as a function of reaction time.

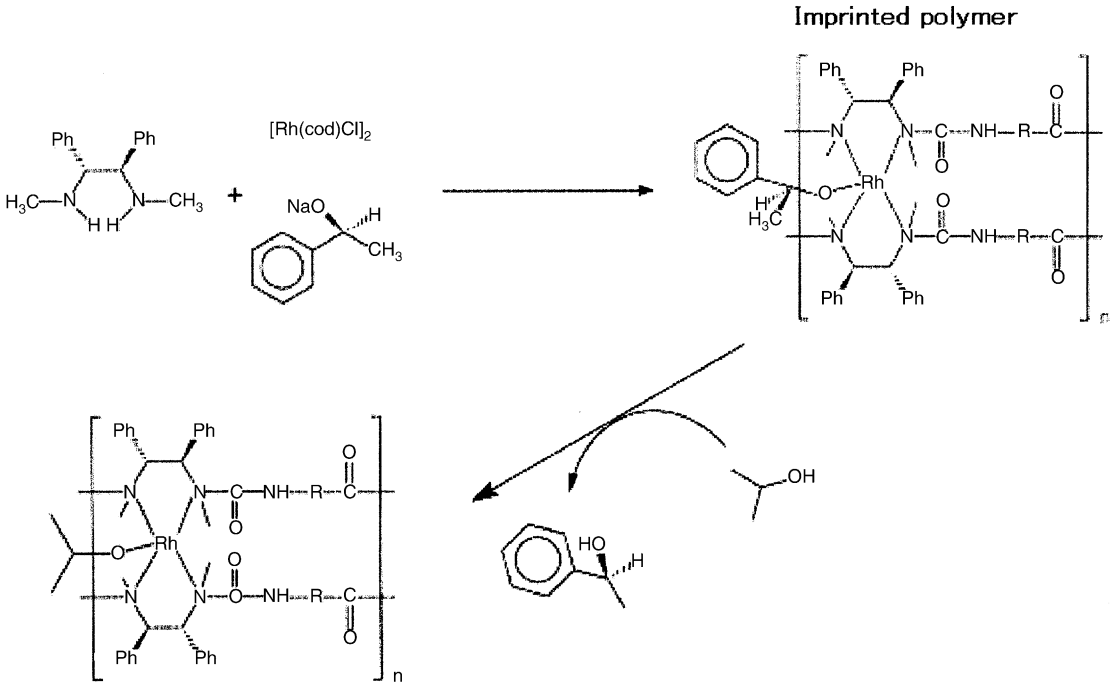

Fig. 5. Preparation steps for polyurea-attached rhodium catalyst by molecular imprinting.

catalytic systems, difference in polymers, cross-linking ratio, and template chirality.

The homogeneous catalyst in solution converted acetophenone to (*R*)-phenyl ethanol in 7 days and enantio excess was 67%. In the case of non-imprinted polymer acetophenone was converted to (*R*)-phenyl ethanol with 25% enantio excess and phenyl ethyl ketone to (*R*)-phenyl propanol with 47%. Enantio excess increased to 60% by changing polymer matrices and cross-linking ratios. In contrast, acetophenone was quantitatively reduced to (*S*)-phenyl ethanol in 1 day and enantio excess was 60%. On the other hand, acetophenone was converted to (*R*)-phenyl ethanol with 43% enantio excess and phenyl ethyl ketone to (*R*)-phenyl propanol with 66% on the (*R*)-template imprinted polymer (same polymer matrix as the above non-imprinted polymer) as shown in Table 3. The enantio excesses on the imprinted polymer were higher than that on the non-imprinted polymer and (*R*)-product was obtained by the (*R*)-template imprinted polymer. However, in the case of another polymer backbone, both (*R*)- and (*S*)-template imprinted polymers produced (*S*)-phenyl ethanol from acetophenone, therefore, chiral conformation of produced alcohol was suggested to be influenced by structures of chiral polymers not by conformation of the used template. In addition to examination of relation between template conformation and enantio excess, they also

Table 3
Catalytic activities for hydride transfer reduction of acetophenone and ethyl phenyl ketone

Reactant	Catalyst	Inductor configuration	Conversion (%)	Time (day)	ee (*R*) (%)
Acetophenone	Polymerized	(*S*,*S*)	98	1	25
Acetophenone	(*R*)-Templated	(*S*,*S*)	98	1	43
Ethyl phenyl ketone	Polymerized	(*S*,*S*)	96	6	47
Ethyl phenyl ketone	(*R*)-Templated	(*S*,*S*)	91	9	66

Table 4
Hydride transfer reduction of different ketones on the imprinted Rh polymer

Reactant	Imprinted polymer		Non-imprinted polymer	
	Initial rate (mmol h^{-1} g^{-1} per Rh)	ee (*R*) (%)	Initial rate (mmol h^{-1} g^{-1}per Rh)	ee (*R*) (%)
Ethyl phenyl ketone	18.3	70	1.5	48
Phenyl propyl ketone	14.7	44	5.2	58
4′-Trifluoromethyl acetophenone	64	38	10	30

compared activities for other reactants with different shapes on both non-imprinted and imprinted polymers. The results were summarized in Table 4. Enhancement of reaction rates and size selectivity were observed on the imprinted polymer. The imprinted effect was obvious for molecule related structurally to the template and it is not efficient for the reactant with too different structure from the template.

Another asymmetric transfer hydrogenation of ketones was reported by Severin in 2000. Polymer-immobilized ruthenium [46] and rhodium [47] complexes coordinated with phosphinato ligand with similar shape to transition-state-mimicking intermediate of the reaction. Here, we take up studies of ruthenium catalysts for substrate- and regioselective transfer hydrogenation of ketones [46]. The transfer hydrogenation of ketones catalyzed by the half-sandwich complexes of ruthenium coordinated with amine-based ligands has recently received much attention, because of its high activity and enantioselectivity. For this kind of reactions, a six-membered cyclic structure is proposed as an intermediate as shown in Fig. 6(a). An analogue structure of the intermediate can be designed by phosphinato ligand to coordinate ruthenium as shown in Fig. 6(b). Tetrahedral conformation of the phosphinato ligand possesses a similar shape to the reactive carbon center of the six-membered cyclic structure.

Incorporation of ruthenium complex into organic polymer was performed by grafting of styrene side chain of diamine coordinated to Ru center. They prepared monosubstituted and disubstituted diamine

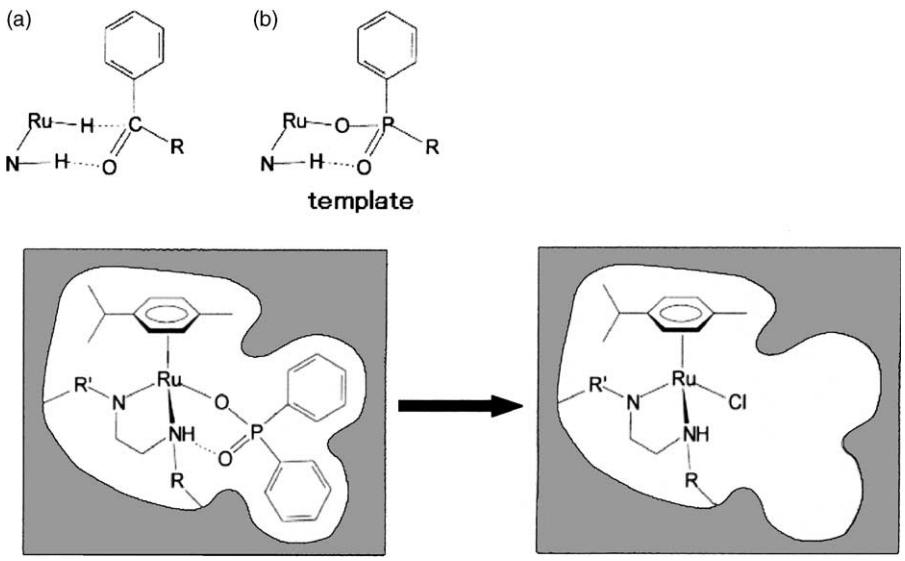

Fig. 6. An intermediate of transfer hydrogenation of ketones on ruthenium complex (a) and its analogue by phosphinate ligand (b). Molecular-imprinting step of the phosphinate template coordinated ruthenium complex in polymer matrix.

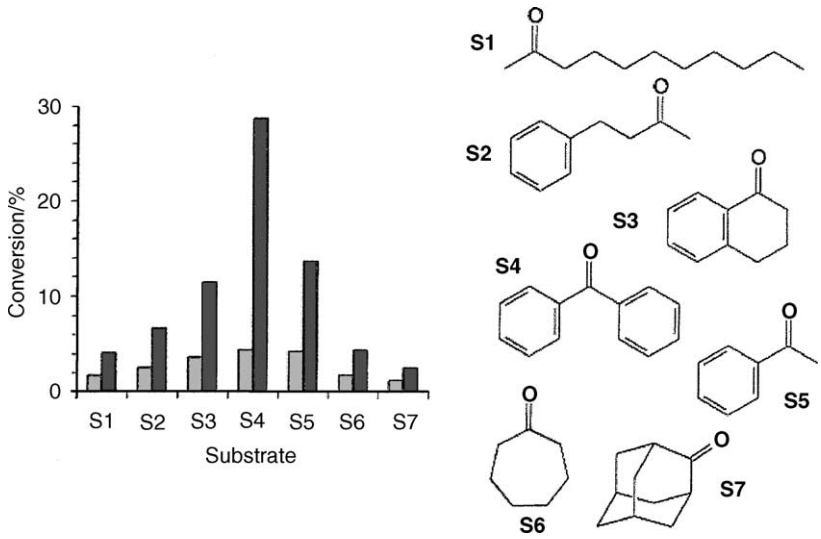

Fig. 7. Yields of competition reaction of transfer hydrogenation of seven ketones with different shapes on the imprinted ruthenium polymer and non-imprinted polymer.

ligands and polymerized ethylene glycol dimethacrylate (EGDMA) with (η^6-arene)Ru complex. The polymer reagent was most popular material in molecular imprinting. After the polymerization, the template phosphinato ligand was removed by treatment with a solution of [$BuNEt_3$]Cl in methanol and replaced by chloro ligand, thereby generating a form-selective cavity (Fig. 6). From ICP measurement, at least 80% of the template is released by this procedure. Reference polymers were also prepared by (η^6-arene)Ru complex coordinated with chloro ligand instead of the template phosphinate ligand. The imprinted polymers were shown to enhance the reaction rates as compared to the polymer prepared without the template. Compared with two pairs of the imprinted and reference polymers (mono-grafted and di-grafted), the latter case exhibited higher rate enhancement (factor of seven), while the former ratio was three. The reason why the latter di-grafted polymer was more active is not clear, but density of the polymer matrix, path of reactant to access to the ruthenium site, and proportion of ruthenium species located at surface of the polymer may give influence to the activity of imprinted polymer. The di-grafted material is considered to have more rigid matrix and reduce its flexibility by connection to the polymer backbone at two points. Conformation around the ruthenium site is suggested to be more restricted than the ruthenium complex in solution and selectivity for benzophenone that has similar shape to the cavity would be observed.

Indeed reaction rate of benzonphenone on the imprinted polymer was higher than other different ketones in competition experiment with equal amount of seven ketones (S1–S7) including benzophenone as shown in Fig. 7. On the contrary, the seven ketones reacted in similar rates on the controlled polymer without the cavity. The enhancement of the reaction rate for benzonphenone was more significant than the other ketones and enhancement of a factor of 6.6 was observed for benzophenone. While the values drops to about 3 for the other ketones, indicating that the imprinted polymer was specific for benzophenone with two phenyl groups. However, all the other ketones have no or only one aromatic ring, and their adsorptions to the polymer are considered to be weaker compared with benzophenone. As the result, the reaction rates of the other ketones would be lower values than that of benzophenone. In case of the reaction of each single reactant, selectivity for the seven ketones might not change so much.

These examples were molecular imprinting of reaction intermediates of metal-complex catalysts in bulk polymers. However, active sites prepared by bulk imprinting are often not uniform and distributed widely

from bulk to surface and different accessible sites were formed in bulk polymer matrices [56]. Therefore, detailed characterization of imprinted sites, structure of metal complexes, size of template cavities, distribution of location of the pores, etc. have not been performed and difficulty of characterization has prevented understanding of mechanism to regulate catalytic reactions at the imprinted sites. Furthermore, location of the imprinted sites inside bulk polymer matrices is difficult for access of reactant molecules to the site than surface-located sites. As a result, the bulk imprinting method may be disadvantageous to prepare active catalyses like natural enzymes where active reaction cavity with metal site is located at the surface/interface of protein bulk.

4. Molecular imprinting of rhodium monomers attached on SiO_2 surface

Imprinting at surfaces can provide catalytic sites readily accessible for reactant molecules and more uniform locations of imprinted sites. Few examples have been reported on acid–base catalysts for amide hydrolysis [40], alkane combustion [41] and ester hydrolysis reactions [42]. However, molecular imprinting at surfaces for metal-complex catalysts had been not reported for a long time before our study. Very recently, we have prepared SiO_2-attached imprinted rhodium catalysts by molecular imprinting on Ox.50 (SiO_2) surface for shape-selective hydrogenation of simple alkenes without any functional group [49–51]. Recognition of simple alkenes without any functional group is generally difficult.

Our approach of surface molecular imprinting for metal-complex catalyst is accomplished by combining two techniques: (1) metal-complex attachment on oxide surface; and (2) molecular imprinting for ligand of the attached metal complex at the surface. From many studies for attached metal complexes, it is known that they may exhibit unique catalytic properties with high activities because of stabilization of coordinatively unsaturated active structures at oxide surfaces and new structures without analogues in homogeneous systems [57–62]. Attachment of metal complexes to oxide surfaces and transformation of the attached metal complexes to active structures at the surfaces are one of the ways to enable to fulfill high activity and maintain such unsaturated active species that decompose easily in solution. The application of molecular-imprinting technique to such attached metal complexes can realize sophisticated regulation beyond simple supported metal-complex catalysts. Our strategy to design active and selective catalysts was based on the following five regulations: (1) conformation of ligands coordinated to Rh atom; (2) orientation of vacant site on Rh; (3) cavity with template molecular shape for reaction space produced behind template removal; (4) architecture of the cavity wall; and (5) micropore in inorganic polymer-matrix overlayers stabilizing the active species at the surface.

Attachment and molecular imprinting for rhodium monomer were performed by following procedure as shown in Fig. 8 [49]. First we prepared a new SiO_2-attached Rh-monomer catalyst (Rh_{sup} catalyst), which has two $P(OCH_3)_3$ ligands per Rh by impregnating $RhCl(P(OCH_3)_3)_3$ precursor on Ox.50 surface and subsequent evacuation at 363 K. Second, we created novel imprinted Rh_{imp} catalysts with template cavity by using one of the two $P(OCH_3)_3$ ligands as template for molecular imprinting (Rh_{imp} catalyst). $P(OCH_3)_3$ possesses methoxy groups which may have positive interaction with $Si(OCH_3)_4$ used as a reagent for imprinting polymerization to make fine template cavities. $P(OCH_3)_3$ was also regarded to be analogue to a half-hydrogenated alkyl intermediate for hydrogenation of 3-ethyl-2-pentene.

Stacking of SiO_2-matrix overlayers for molecular imprinting occurred at the surface, which was characterized by ^{29}Si solid-state MAS-NMR and XPS analyses. Accompanied with stacking of SiO_2-matrix overlayers, XPS Rh 3d peak intensities reduced, indicating that space around the attached Rh complex was covered by the SiO_2 matrix. Stacking of SiO_2-matrix overlayers on the surface changed catalytic activity of the rhodium complex for hydrogenation of 2-pentene and the catalytic activities remarkably depended on heights of the SiO_2-matrix overlayers as shown in Fig. 9. Attended to increase of the heights of SiO_2-matrix overlayers, 2-pentene hydrogenation activities swelled widely and reached 11 times higher activity as compared to that of the supported catalyst (Rh_{sup}) after stacking of SiO_2-matrix overlayers of 3.8 nm height. Further increase in the amount of SiO_2-matrix overlayers reduced the catalytic activity and it became 33% of the maximum activity of the 3.8 nm height sample.

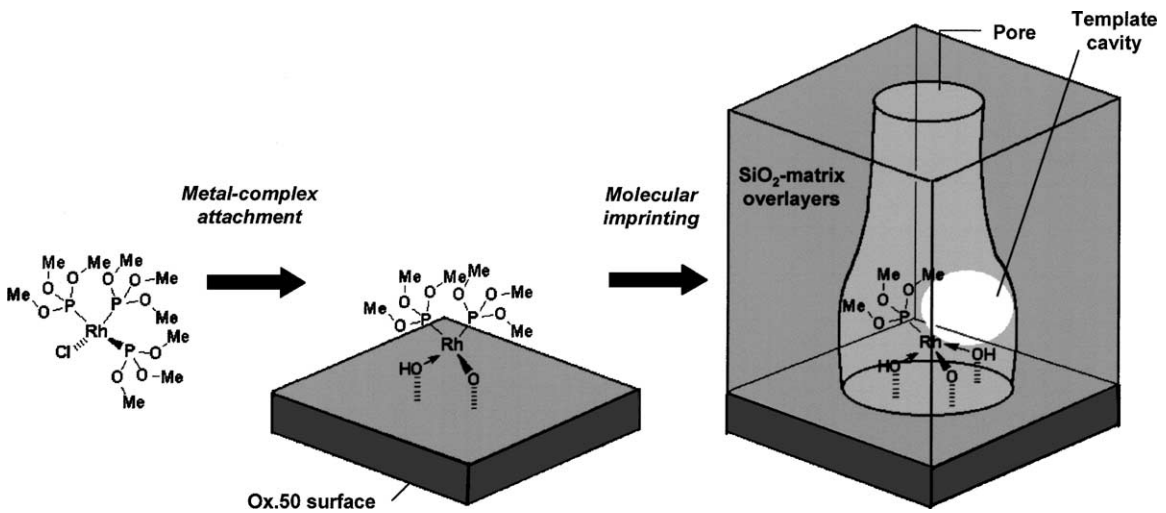

Fig. 8. Synthesis procedure of SiO_2-attached rhodium monomer catalyst by metal-complex attachment and subsequent surface molecular imprinting.

The increase of hydrogenation activities corresponded to change of surface-attached rhodium structure, which was demonstrated by EXAFS analysis. Fig. 10 and Table 5 show Rh K-edge EXAFS Fourier transforms and their curve-fitting results for the supported and imprinted rhodium catalysts with different heights of SiO_2-matrix overlayers. The curve-fitting results demonstrate that the structure around Rh atoms in the imprinted catalysts is different from that for the supported catalyst before the imprinting. The Rh monomers with the SiO_2-matrix overlayers of 3.8 and 6.4 nm were characterized to be coordinated with one $P(OCH_3)_3$ and three surface oxygens as illustrated in Fig. 8. The reduction of the coordination number (CN) of Rh–P bond signified that removal of a template ligand $P(OCH_3)_3$ per Rh occurred in the imprinting step. The removal of one of the two $P(OCH_3)_3$ ligands by the surface imprinting provides the cavity of the template shape for reaction space as illustrated in Fig. 8. The increase of hydrogenation activities may be due to formation of the coordinatively unsaturated structure. Thus the imprinting provided the active monomer structure with the template cavity as reaction site.

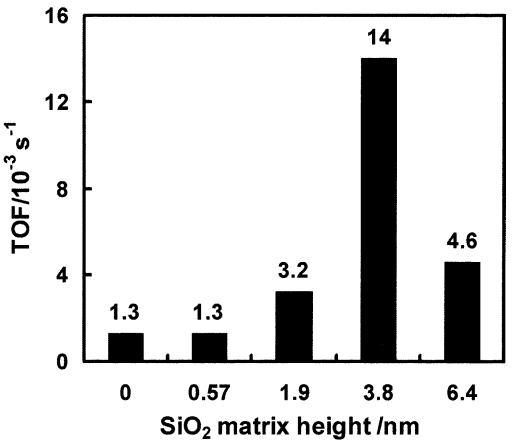

Fig. 9. TOF for hydrogenation of 2-pentene on the supported and imprinted Rh-monomer catalysts.

Existence of micropores in the SiO_2-matrix overlayers was confirmed by *t*-plots in Fig. 11. There was no break in the *t*-plot for the SiO_2-matrix overlayers without Rh complexes and hence there was no uniform micropores. The supported catalyst without SiO_2-matrix overlayers and the $Rh_{imp\text{-}1.4}$ sample with 1.4 ML (0.57 nm) SiO_2-matrix overlayers were both regarded to be nonporous materials (Fig. 11(a) and (b)). Fig. 11(c–e) represent *t*-plots for the $Rh_{imp\text{-}4.7}$, $Rh_{imp\text{-}9.3}$ and $Rh_{imp\text{-}15.9}$ catalysts with SiO_2-matrix overlayers of 1.9, 3.8 and 6.4 nm, respectively, which demonstrate formation of micropores by the imprinting. The micropore diameters were estimated to be 0.67, 0.64 and 0.60 nm, for the $Rh_{imp\text{-}4.7}$, $Rh_{imp\text{-}9.3}$

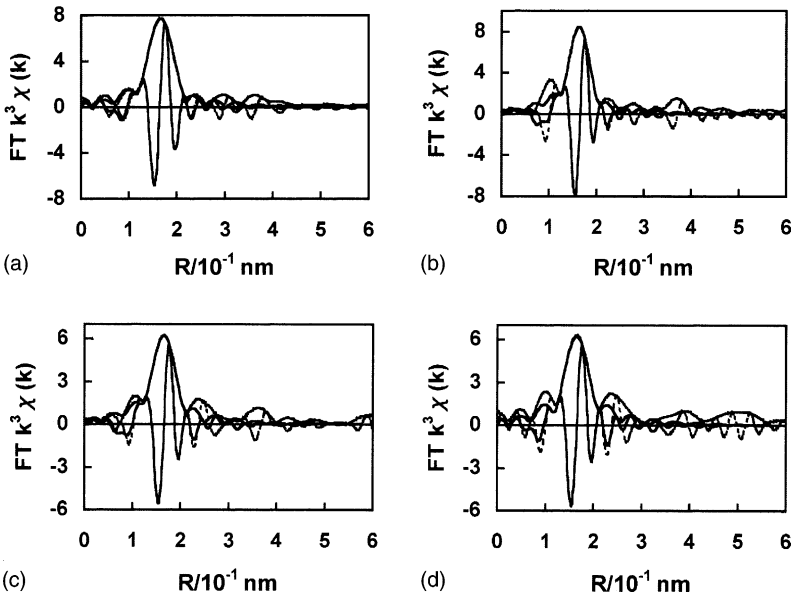

Fig. 10. The k^3-weighted Rh K-edge EXAFS Fourier transforms for the supported and imprinted Rh-monomer catalyst: (a) Rh_{sup} catalyst; (b) $Rh_{imp\text{-}4.7}$ catalyst; (c) $Rh_{imp\text{-}9.3}$ catalyst; and (d) $Rh_{imp\text{-}15.9}$ catalyst.

and $Rh_{imp\text{-}15.9}$ catalysts, respectively. The pore sizes were estimated to be about 75% of the size of $[Rh(P(OCH_3)_3)_2]$ precursor by DFT as illustrated in Fig. 8. The active $Rh_{imp\text{-}9.3}$ catalyst was air-stable and highly durable for the catalytic hydrogenation due to the location and chemical attachment of the Rh monomers at the bottom in the micropores of the SiO_2-matrix overlayers on the Ox.50 surface.

The large ligand $P(OCH_3)_3$ of the Rh monomer can regulate the reactivity of the metal center

Table 5
Structural parameters derived from EXAFS curve-fitting analysis for the supported and imprinted Rh-monomer catalysts[a]

Shell	CN[b]	R (nm)	σ^2 (nm^2)	
0 ML[c]				
Rh–O	1.8 ± 0.7	0.204 ± 0.002	$(5 \pm 1) \times 10^{-5}$	$\Delta E_0 = 6 \pm 5$ eV
Rh–P	2.2 ± 0.7	0.225 ± 0.002	$(6 \pm 2) \times 10^{-5}$	$R_f = 0.03\%$
4.7 ML[d]				
Rh–O	2.5 ± 0.6	0.205 ± 0.002	$(3 \pm 2) \times 10^{-5}$	$\Delta E_0 = 5 \pm 3$ eV
Rh–P	1.5 ± 0.6	0.223 ± 0.001	$(7 \pm 4) \times 10^{-5}$	$R_f = 0.07\%$
9.3 ML[c]				
Rh–O	2.8 ± 0.3	0.208 ± 0.001	$(9 \pm 2) \times 10^{-5}$	$\Delta E_0 = 8 \pm 2$ eV
Rh–P	1.2 ± 0.3	0.225 ± 0.001	$(4 \pm 1) \times 10^{-5}$	$R_f = 0.04\%$
15.9 ML[c]				
Rh–O	2.9 ± 0.2	0.210 ± 0.004	$(9 \pm 4) \times 10^{-5}$	$\Delta E_0 = 11 \pm 5$ eV
Rh–P	1.1 ± 0.2	0.225 ± 0.001	$(1 \pm 3) \times 10^{-5}$	$R_f = 0.3\%$

[a] EXAFS spectra were measured at 15 K.
[b] Summation of the CN of Rh–O and Rh–P was fixed as 4.0 for the curve fitting.
[c] The k range and the R range were 30–100 nm^{-1} and 0.12–0.21 nm, respectively.
[d] The k range and the R range were 30–110 nm^{-1} and 0.12–0.21 nm, respectively.

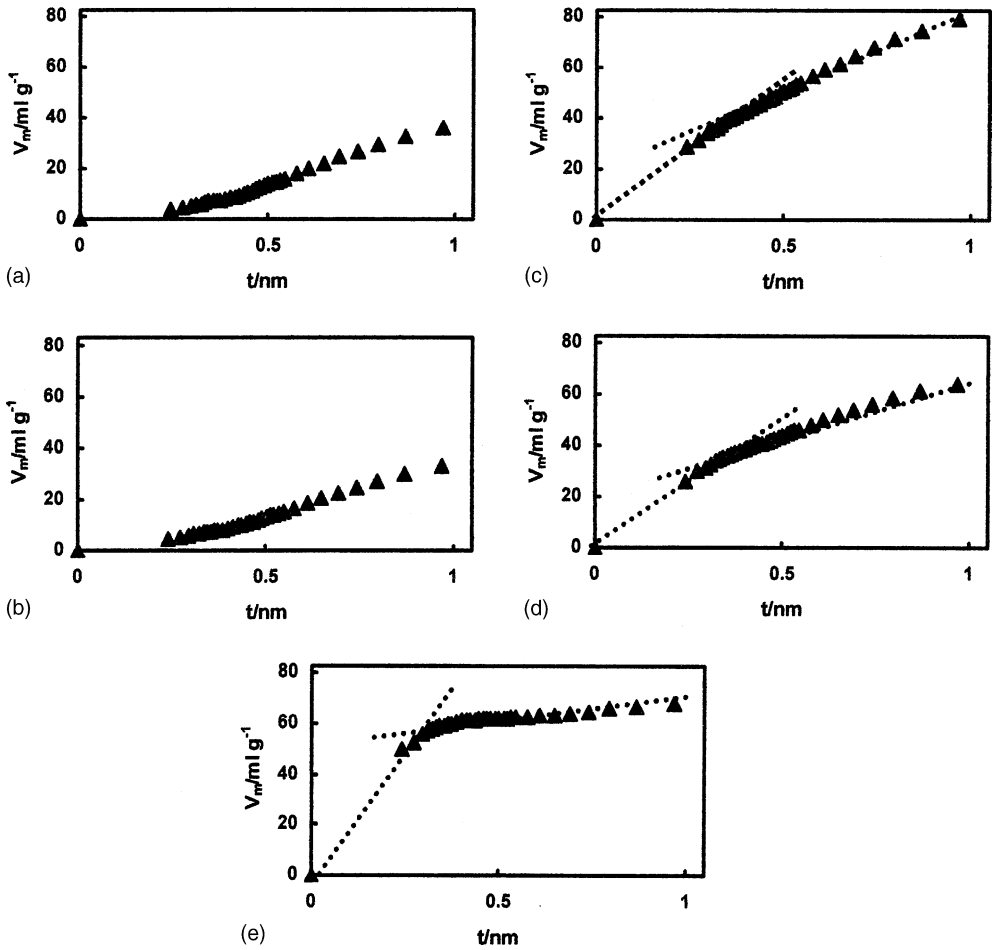

Fig. 11. BET *t*-plots for the supported and imprinted Rh-monomer catalysts: (a) Rh_{sup} catalyst; (b) $Rh_{imp\text{-}1.4}$ catalyst; (c) $Rh_{imp\text{-}4.7}$ catalyst; (d) $Rh_{imp\text{-}9.3}$ catalyst; and (e) $Rh_{imp\text{-}15.9}$ catalyst.

electronically and geometrically to give higher selectivity than metal and metal oxide catalysts without any ligand. The selectivity of the surface-attached Rh monomers is also subjected to regulation by the surface which is regarded as a unique and large ligand. The supported Ru_{sup} catalyst showed high selectivity for the alkene hydrogenation as shown in Table 6. The rate of 2-pentene hydrogenation was 16 and 8 times faster than those of 3-methyl-2-pentene and 4-methyl-2-pentene, respectively. In contrast to the branch alkenes, length of the alkene main chain did not affect the reaction rates negatively (2-pentene, 2-hexene, 2-heptene, and 2-octene).

Selectivity for the alkene hydrogenation on the imprinted catalyst depended on the size and shape of the template cavity as reaction site in the micropores of the SiO_2-matrix overlayers on the Ox.50 surface in addition to the electronic and geometric effects of the ligands of the Rh complex. To examine the molecular-imprinting effect on the selectivity, we compared the ratios of turnover frequencies (TOF) of the imprinted catalyst to TOF of the supported catalyst for each alkene. There existed the difference in the TOF ratios between the C_5 and C_6 alkenes and the C_7 and C_8 alkenes and the difference in the rate enhancement by the imprinting

Table 6
Catalytic activities of the imprinted Rh-monomer catalyst, degrees of the enhancement of the reaction rates by molecular imprinting (ratios of TOF), activation energies (E_a), activation enthalpies ($\Delta^{\ddagger}H$) and activation entropies ($\Delta^{\ddagger}S$) for the catalytic hydrogenation of alkenes[a]

Reactant	Imprinted catalyst TOF (s^{-1})	Ratio of TOF[b]	Supported catalyst			Imprinted catalyst		
			E_a ($kJ\,mol^{-1}$)	$\Delta^{\ddagger}H$ ($kJ\,mol^{-1}$)	$\Delta^{\ddagger}S$ ($J\,mol^{-1}\,K^{-1}$)	E_a ($kJ\,mol^{-1}$)	$\Delta^{\ddagger}H$ ($kJ\,mol^{-1}$)	$\Delta^{\ddagger}S$ ($J\,mol^{-1}\,K^{-1}$)
C_5								
2-Pentene	1.4×10^{-2}	11	35	32	−202	33	30	−188
C_6								
3-Methyl-2-pentene	1.1×10^{-3}	13	42	39	−205	38	35	−195
4-Methyl-2-pentene	1.1×10^{-3}	6.9	38	35	−211	41	38	−186
2-Hexene	1.7×10^{-2}	6.5	29	26	−213	27	24	−203
C_7								
3-Ethyl-2-pentene	1.2×10^{-4}	3.4	43	40	−209	11	8	−291
3-Methyl-2-hexene	3.6×10^{-5}	–	[c]	[c]	[c]	13	10	−295
4-Methyl-2-hexene	1.2×10^{-4}	2.4	43	40	−206	9	6	−296
2-Heptene	7.1×10^{-3}	3.9	31	28	−211	11	8	−257
C_8								
2-Octene	8.8×10^{-3}	2.8	29	26	−212	10	7	−259

[a] Rh/alkene/toluene = 1/1000/23,000; H_2 = 101.3 kPa.
[b] TOF of the $Rh_{imp\text{-}9.3}$ catalyst/TOF of the Rh_{sup} catalyst, at 348 K.
[c] Negligible TOF.

is due to the difference in size and shape of the alkenes.

The difference in the TOF ratios between 3-methyl-2-pentene and 3-ethyl-2-pentene was so large, where the difference in the length of the branch group between methyl and ethyl is discriminated on the imprinted catalyst. The difference in the branch groups between methyl and ethyl was also observed for the hydrogenation of 4-methyl-2-pentene and 4-methyl-2-hexene. The TOF ratio for 4-methyl-2-hexene was much smaller than that for 2-pentene, where the alkenes have difference in the size and shape of the ethyl group. There was also a big difference between 2-pentene and 2-heptene, where an ethyl group of alkene main chain could be discriminated. Thus, the molecular-imprinting catalyst can discriminate the size and shape of the alkenes without functional groups. It is noteworthy that the reaction rates of the linear alkenes such as 2-pentene, 2-hexene, 2-heptene and 2-octene on the supported Rh_{sup} catalyst were similar to each other, whereas on the imprinted $Rh_{imp\text{-}9.3}$ catalyst the rate enhancements (TOF ratios) for 2-hepente and 2-octene (3.9 and 2.8 times, respectively) were much less than those for 2-pentene and 2-hexene (11 and 6.5 times, respectively). Because the length of linear alkene chains could not be discerned by ligand-coordinated metal site in the supported Rh_{sup} catalyst, it is concluded that the difference was caused by the space and shape of the template cavity at the imprinted Rh-monomer site.

It is well known that hydrogenation mechanism involves four steps; dissociation of hydrogen molecule on metal center to form hydrides, coordination of alkene C=C double bond to the metal center, insertion to the Rh–H bond to form a half-hydrogenated alkyl species, and final reaction of the alkyl with remaining hydride. The rate-determining step has been experimentally and theoretically considered to be the third step (alkyl formation). The activation energies for the alkene hydrogenation on the supported catalyst before the imprinting, ca. 30 and 40 $kJ\,mol^{-1}$ for linear alkenes and branch alkenes, respectively, in Table 6 are typical values for the activation energies on metal-complex catalysts. The activation entropies for the catalytic hydrogenation on the supported catalyst were similar values for all the alkenes used in this study (Table 6). The activation energies and activation entropies for the hydrogenation of the C_5 and C_6 alkenes did not change significantly after the imprinting (Table 6). These results demonstrate that

the rate-determining step for the hydrogenation of the smaller C_5 and C_6 alkenes than the template on the supported and imprinted catalysts is the same as that for the Wilkinson complex catalyst and the catalytic hydrogenation of the smaller alkenes is not regulated by the template cavity.

In contrast, the activation energies for the larger C_7 and C_8 alkenes with different shapes from the template $P(OCH_3)_3$ on the imprinted $Rh_{imp\text{-}9.3}$ catalyst were so small as 9–13 kJ mol^{-1}. These dramatic decrease in the activation energy together with the small TOF ratios (less promotion) discussed above, indicates shift of the rate-determining step from the alkyl formation to π-coordination of alkene to Rh. Accompanied with this shift, the activation entropies for the hydrogenation of those alkenes also decreased largely to −257 to −295 from −206 to −212 J mol^{-1} K^{-1} for the Rh_{sup} catalyst. The values of −257 to −295 J mol^{-1} K^{-1} were also much smaller than the values of −186 to −203 J mol^{-1} K^{-1} for the smaller alkenes as shown in Table 6. The decrease in the activation entropy suggests that conformation of the coordinated alkene in the template cavity is strongly regulated by shape of the template cavity and the remaining $P(OCH_3)_3$ ligand. For the C_7 and C_8 alkenes with the larger sizes and different shapes, it is concluded that the regulation of the alkene hydrogenation occurs on the step of alkene coordination to the imprinted Rh monomer due to the different size and shape of the alkenes sticking out of the template cavity. It is to be noted that the shape of alkenes without any functional group was discriminated on the imprinted catalyst, which was successfully prepared by the molecular imprinting of metal–monomer complex on oxide surface.

5. Molecular imprinting of rhodium-dimers attached on SiO_2 surface

We have also prepared a new Rh-dimer molecular-imprinting catalyst (Rh_{2imp}) at SiO_2 surface for hydrogenation of alkenes, whose procedure is presented in Fig. 12 [50,51]. The metal dimer was regarded as a minimum active structure for heterogeneous metal

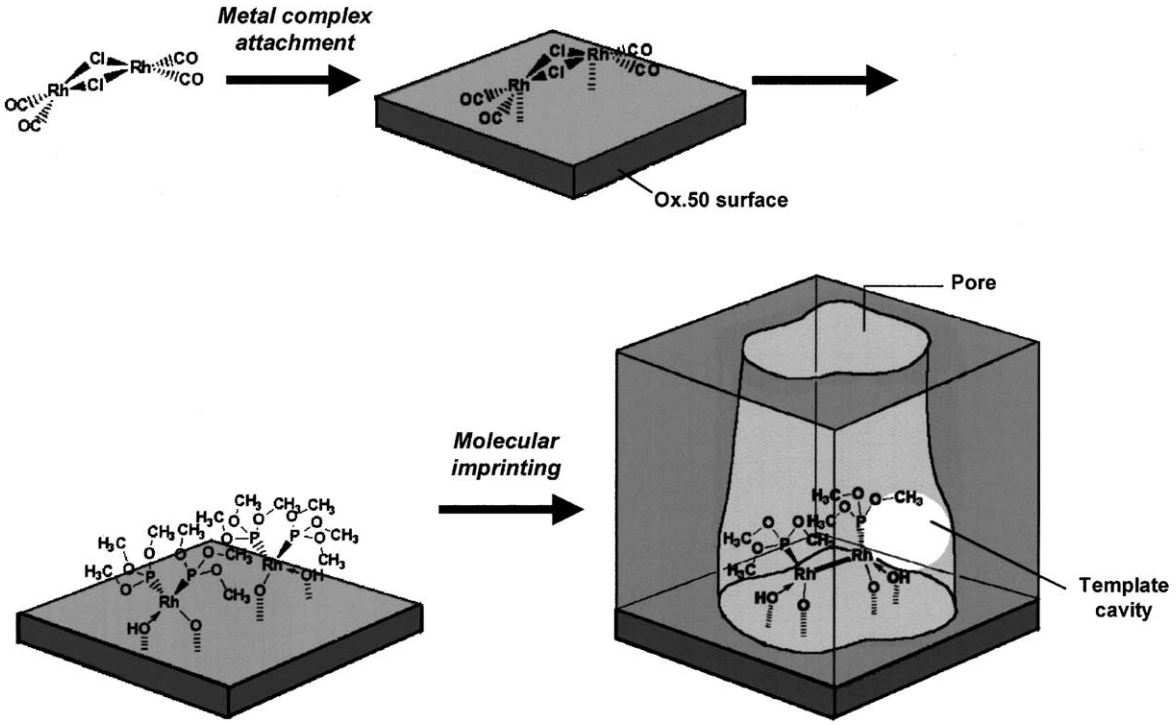

Fig. 12. Preparation steps for imprinted Rh-dimer catalyst on SiO_2 surface.

catalysts involving metal–metal bonding. Bridged Rh-dimer precursor $Rh_2Cl_2(CO)_4$ was attached on SiO_2 surface and exposed to $P(OCH_3)_3$ to make rhodium–phosphite complex at the surface. The phosphite ligand was used as template molecule for a half-hydrogenated alkyl intermediate of hydrogenation of 3-ethyl-2-pentene. Polymerization of $Si(OCH_3)_4$ on the surface in the presence of H_2O generated cavity with the molecular size of the template at the Rh site in SiO_2-matrix overlayers. We have also characterized the attached Rh dimer, the Rh phosphite complex, and the imprinted Rh structure at the SiO_2 surface by means of elemental analysis, FT-IR, XPS, ICP, solid-state MAS-NMR, BET, and EXAFS [50].

$Rh_2Cl_2(CO)_4$ was used as precursor and attached at the surface retaining its dimer structure. From results of EXAFS and XPS analyses, the surface-attached Rh dimer was converted to supported Rh-monomer pair (Rh_{2sup}) with two $P(OCH_3)_3$ ligands at 0.224 nm and two oxygens at 0.203 nm per Rh. Molecular imprinting for the attached rhodium complexes was performed by polymerization of $Si(OCH_3)_4$ too, which possesses methoxy groups with positive interaction between the template. Accompanied with the imprinting on the surface, XPS intensity of Rh 3d reduced widely as shown in Fig. 13. The surface imprinting caused dimerization of the Rh monomers and removal of the template ligand. As the result, highly active Rh dimers were created in the 0.74 nm pores in the SiO_2-matrix overlayers. The imprinted catalyst had a direct Rh–Rh bond at 0.268 (±0.001) nm with the CN of 1.3 (±0.3) nm. It is suggested that dimerization of two adjacent Rh monomers occurred inside the SiO_2-matrix overlayers. Furthermore, the CN of Rh–P bond at 0.221 (±0.001) nm reduced from 2.3 (±1.4) to 1.1 (±0.2) nm, which indicates that a phosphite ligand per Rh was eliminated during the dimerization. The Rh dimer with a $P(OCH_3)_3$ ligand on each Rh atom was stabilized at the Ox.50 surface through Rh–O bonding at a distance of 0.211 (±0.002) nm. The Rh attaching on the surface in a bidentate form (CN of Rh–O bonds: 2.0±0.5 in Table 7) is similar to that for the supported Rh monomers (1.6 ± 1.0). At one of two Rh atoms in the dimer the template-size cavity was produced and combined with the pore, which is illustrated in Fig. 12.

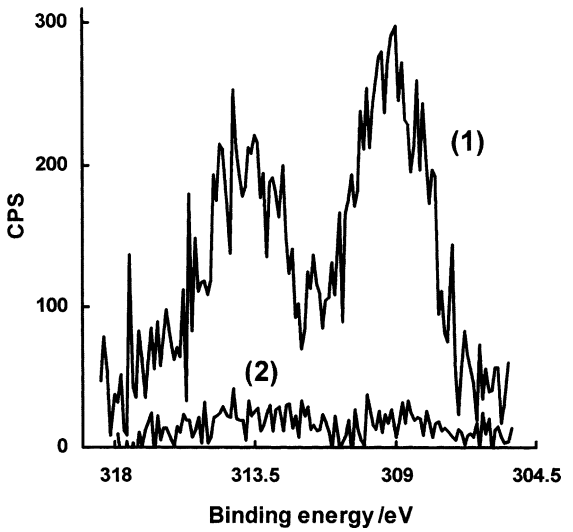

Fig. 13. Rh 3d XPS spectra for the supported (1) and imprinted (2) Rh-dimer catalysts. Rh 3d peaks were normalized by each Si 2p peak intensity.

Mechanism of the change in Rh structures and structure of imprinted Rh species in the imprinting process were examined by DFT calculation. Five structural models on a silica cluster substrate, $[Rh(P(OCH_3)_3)_2]_2$, $Rh(P(OCH_3)_3)$–$Rh(P(OCH_3)_3)_2$, $Rh_2(P(OCH_3)_3)_3$, P-bridged $Rh_2(P(OCH_3)_3)_3$ and $Rh_2(P(OCH_3)_3)_2$, were calculated, which are regarded as models for the Rh-monomer pair catalyst (Rh_{2sup}), possible intermediate species with three $P(OCH_3)_3$ ligands and the imprinting Rh-dimer catalyst (Rh_{2imp}). The optimized structure, structural parameters and relative stability for those model species are illustrated in Fig. 14. During the optimization processes, the SiO_2 substrate was fixed after the change in total energy became $<0.5\,kcal\,mol^{-1}$, since positions of silicon atoms and oxygen atoms in the substrate exhibited no significant change in this regime. Initial structure of each Rh complex including the SiO_2 substrate was obtained by molecular mechanics (MM) method with the universal force field 1.02. $[Rh(P(OCH_3)_3)_2]_2$ with four $P(OCH_3)_3$ ligands per two Rh atoms was found to be the most stable complex with a Rh–Rh distance of 0.306 nm, which is indicative of no direct bonding between Rh atoms. $Rh_2(P(OCH_3)_3)_3$ with three $P(OCH_3)_3$ ligands per two Rh atoms was the second most stable complex with a Rh–Rh distance of 0.271 nm corresponding to the formation of Rh–Rh bond. This result implies

Table 7
Structural parameters determined by EXAFS curve-fitting analysis for the imprinted Rh-dimer catalysts (Rh_{2imp})[a]

Shell	CN	R (10^{-1} nm)	σ^2 (10^{-2} nm^2)	
Fresh imprinted catalyst				
Rh–O	2.0 ± 0.5	2.11 ± 0.02	(4 ± 3) × 10^{-3}	$\Delta E_0 = 11 \pm 2$ eV
Rh–P	1.1 ± 0.2	2.21 ± 0.01	(1 ± 2) × 10^{-3}	$R_f = 0.3\%$
Rh–Rh	1.3 ± 0.3	2.68 ± 0.01	(7 ± 1) × 10^{-3}	
After H_2 adsorption				
Rh–O	1.7 ± 0.5	2.08 ± 0.03	(6 ± 3) × 10^{-3}	$\Delta E_0 = 9 \pm 4$ eV
Rh–P	1.2 ± 0.2	2.20 ± 0.01	(2 ± 4) × 10^{-3}	$R_f = 1.6\%$
Rh–Rh	1.3 ± 0.4	2.65 ± 0.01	(7 ± 2) × 10^{-3}	
After reaction of the H_2-adsorbed sample with 3-methyl-2-pentene				
Rh–O	2.2 ± 0.6	2.12 ± 0.03	(5 ± 4) × 10^{-3}	$\Delta E_0 = 12 \pm 3$ eV
Rh–P	1.1 ± 0.2	2.21 ± 0.01	(1 ± 4) × 10^{-3}	$R_f = 1.4\%$
Rh–Rh	1.2 ± 0.4	2.70 ± 0.01	(6 ± 2) × 10^{-3}	

[a] EXAFS spectra were measured at 15 K.

that the desorption of one phosphite ligand is compensated by the formation of Rh–Rh bond. In order to gain insight to this process, one of four $P(OCH_3)_3$ ligands in $[Rh(P(OCH_3)_3)_2]_2$ was removed, while the Rh–Rh bond was fixed at 0.306 nm. The optimized structure with the Rh–Rh bond fixed at 0.306 nm showed the unstable state (Fig. 14). The energy difference (47 kcal mol^{-1}) is roughly estimated to be the

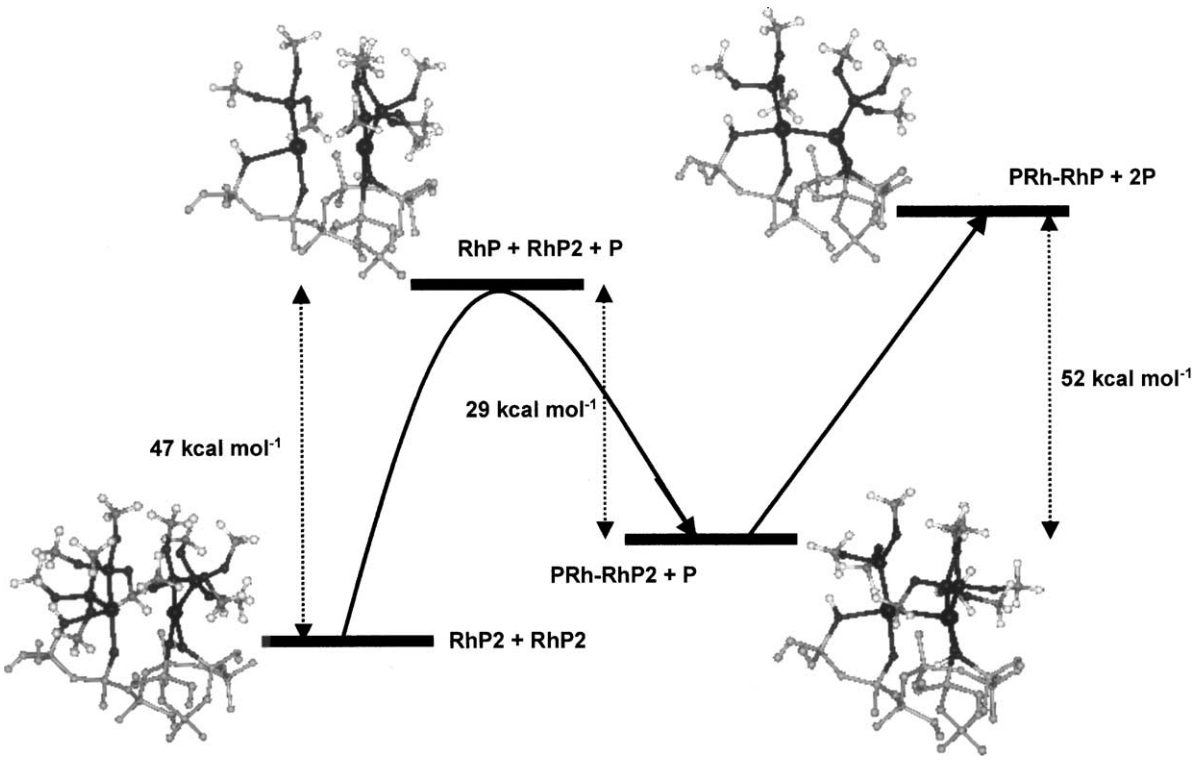

Fig. 14. Energy profile of imprinting step to form active Rh-dimer possessing Rh–Rh bond from Rh-monomer pair estimated by DFT calculations.

activation energy of the ligand desorption process, but the real transition state may involve Rh–Rh bonding at the shorter distance than 0.306 nm, resulting in a decrease in the activation energy. It is to be noted that during the transformation of the supported Rh catalyst to the imprinted Rh catalyst there is a stable structure of $Rh_2(P(OCH_3)_3)_3$ with one phosphite ligand on a Rh atom and with two phosphite ligands on another Rh atom. In order to examine the possibility that the third phosphite ligand interacts with two rhodium atoms, namely, the bridge bonded structure, the initial structure of $Rh_2(P(OCH_3)_3)_3$ with one $P(OCH_3)_3$ bridge bonded was made by the MM method and optimized by the DFT calculation. It was found that this species was unstable by 14 kcal mol^{-1} compared to the non-bridged $Rh_2(P(OCH_3)_3)_3$. Further loss of one of the two $P(OCH_3)_3$ ligands on a Rh atom leads to the formation of $Rh_2(P(OCH_3)_3)_2$ (Rh_{2imp} catalyst). The total energy was further unfavored because of the unsaturated coordination for rhodium atoms (Fig. 14).

The driving force of the loss of a $P(OCH_3)_3$ ligand from $[Rh(P(OCH_3)_3)_2]_2$ and the dimerization of the two adjacent Rh monomers on the Ox.50 surface may be ascribed to the formation of the SiO_2-matrix overlayers surrounding the Rh species. We assume that the elimination of the two phosphite ligands from the monomer pair to produce the $Rh_2(P(OCH_3)_3)_2$ structure (Rh_{2imp} catalyst) occurs step by step via the stable intermediate $Rh_2(P(OCH_3)_3)_3$ with one $P(OCH_3)_3$ on a Rh atom and with two $P(OCH_3)_3$ on another Rh atom in the dimer at the Rh–Rh bond of 0.271 nm. Therefore, the stable intermediate $Rh_2(P(OCH_3)_3)_3$ is the imprinted Rh species under the CVD process at 348 K. In this case the elimination of a template $P(OCH_3)_3$ ligand from the intermediate at 363 K under vacuum generates the template size cavity in the SiO_2-matrix overlayers.

We consider that the good imprinting is achieved by positive interaction between $P(OCH_3)_3$ and $Si(OCH_3)_4$ and the appropriate imprinting conditions. In the CVD process of TMOS and water they would condense around the Rh-monomer pairs on the Ox.50 surface with preferable interaction between both methoxy groups at room temperature. Subsequent heating at 348 K promotes the hydrolysis polymerization of $Si(OCH_3)_4$ to form SiO_2 network around the Rh-monomer pairs. Under this condition, the elimination of a $P(OCH_3)_3$ ligand from either of the two Rh monomers occurs to produce the $Rh_2(P(OCH_3)_3)_3$ dimer intermediate, which is thus imprinted in the SiO_2-matrix overlayers. At this stage the 0.74 nm pores are formed. In the evacuation process at 363 K for 12 h, one $P(OCH_3)_3$ ligand of the two $P(OCH_3)_3$ ligands on a Rh atom in the dimer is desorbed to produce the template-size cavity which is connected to the 0.74 nm micropore. As the result, the reaction space with the similar size to the template $P(OCH_3)_3$ is imprinted on a Rh atom of the dimer in the SiO_2-matrix overlayers on the Ox.50 surface as shown in Fig. 12.

It was found that the imprinted Rh_{2imp} catalyst was tremendously active for alkene hydrogenation. For example, hydrogenation of 3-methyl-2-pentene was promoted 35 times as compared to that on the supported Rh catalyst. Structures around Rh atoms in the Rh_{2imp} catalyst at each step of the alkene hydrogenation were investigated by EXAFS. EXAFS spectra for three samples, fresh Rh_{2imp} catalyst, Rh-dimer hydride species formed by adsorption of 101.3 kPa of H_2 at room temperature, and sample after reaction of the hydride species with 3-methyl-2-pentene at 348 K for 5 min, were measured at 15 K.

The adsorption of hydrogen to produce the monohydride species was irreversible. The second and third adsorptions coincide with each other, which demonstrates the existence of reversible H_2 adsorption. By subtracting the reversible H_2 adsorption from the total H_2 adsorption, the amount of irreversible H_2 adsorption was estimated to be $0.92H_2$/Rh dimer. Thus, most of the Rh sites in the Rh_{2imp} catalyst are converted to have monohydride ligand at saturation of H_2 adsorption.

Because the monohydride complex could maintain the hydride ligand under vacuum, fortunately, structural parameters for the Rh complex, which are equal to those for the Rh complex in situ under H_2 atmosphere, were determined by EXAFS measured at 15 K (Fig. 15) [51]. Fig. 15 shows k^3-weighted EXAFS oscillations and their associated Fourier transformed spectra at Rh K-edge for the three samples and the determined structural parameters are given in Table 7. The Rh dimer after H_2 adsorption exhibited similar EXAFS oscillation and Fourier transform to those of the fresh imprinted catalyst. The detailed analysis of the EXAFS data confirmed retention of local conformation of the Rh dimer with a Rh–Rh bond (CN: 1.3 ± 0.4), two Rh–O bonds (CN: 1.7 ± 0.5) and a

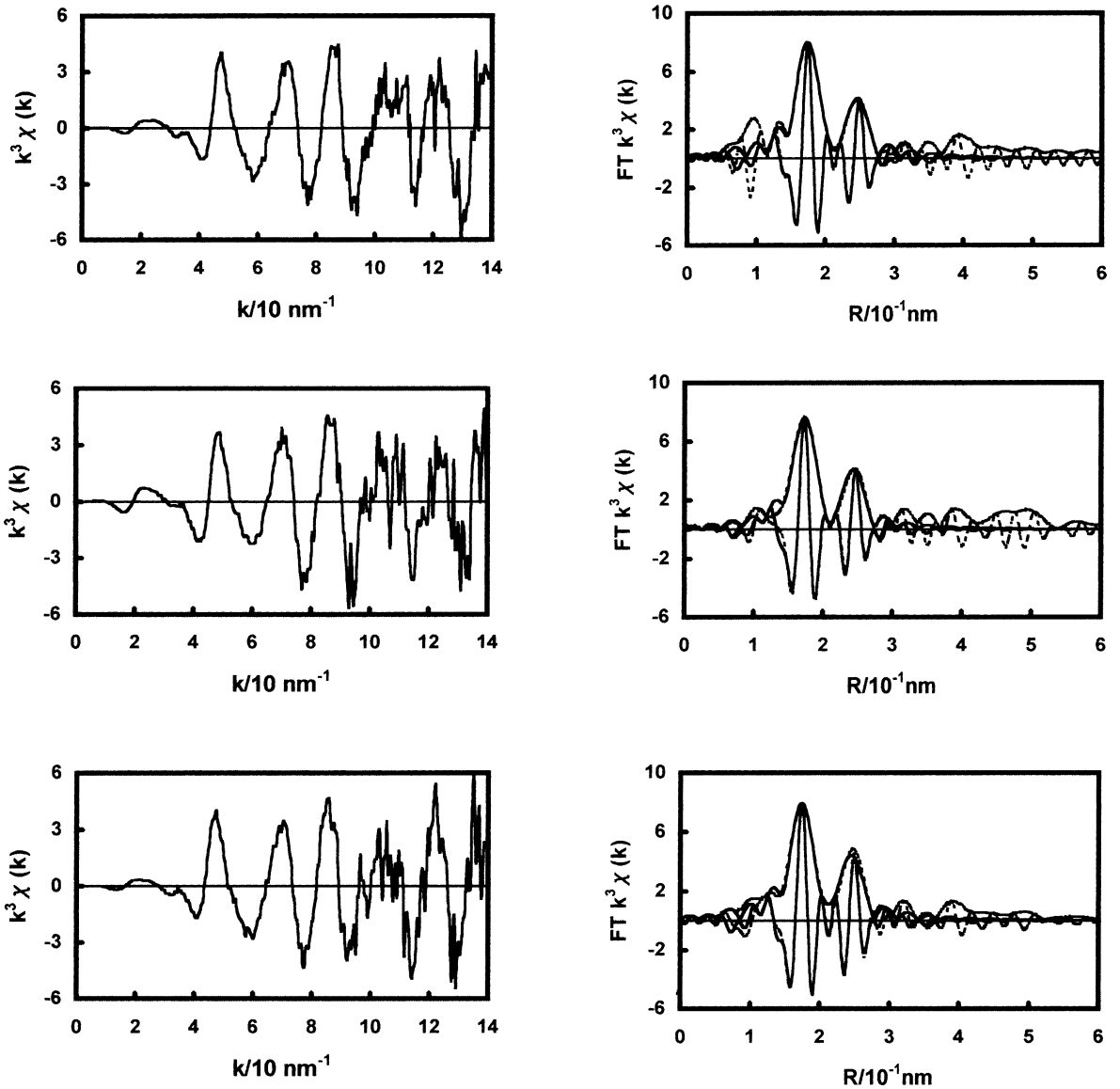

Fig. 15. The k^3-weighted EXAFS oscillations at Rh K-edge and its associated Fourier transforms for the imprinted Rh-dimer catalysts: (top) fresh Rh_{2imp} catalyst; (middle) after hydrogen adsorption; and (bottom) after reaction with 3-methyl-2-pentene at 348 K on the hydrogen-adsorbed Rh_{2imp} catalyst.

Rh–P bond (CN: 1.2 ± 0.2). But contraction of Rh–Rh bond from 0.268 (± 0.001) to 0.265 (± 0.001) nm was found with the hydride dimer, which indicates stabilization of the dimer structure by electronic rearrangement due to hydride coordination on both Rh atoms in the dimer. After reaction of the Rh-dimer hydride species with 3-methyl-2-pentene, the shrunk Rh–Rh bond of the monohydride species expanded again to recover the initial bond length (0.270 ± 0.001 nm). During the hydrogenation process, the Rh–Rh bond was retained without any breaking of the bond. Further, the bond distances and CNs for Rh–O and Rh–P did not change significantly (Table 7). The EXAFS analysis demonstrates that the alkene hydrogenation on the

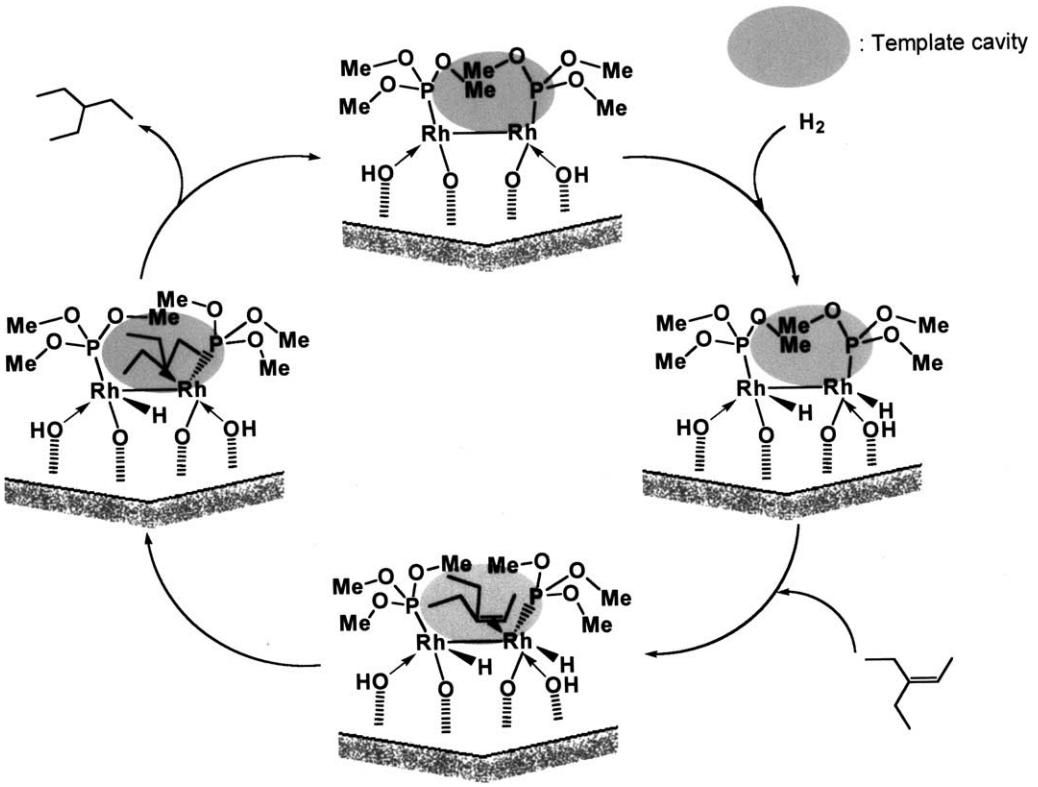

Fig. 16. Mechanism of alkene hydrogenation on the imprinted Rh-dimer catalyst (Rh_{2imp}).

molecular imprinting Rh_{2imp} catalyst proceeds on the Rh-dimer unit in each step of the catalytic cycle. The Rh dimers are attached to the Ox.50 surface through Rh–O bond at 0.211 nm (Table 7). It seems that the chemical attachment in a tetradentate form and the location with stable fitting in the micropore of 1.9 nm thick prevented leaching of the Rh dimers to the reaction solution and decomposing and gathering of the Rh dimers. Associated mechanism of hydrogenation of alkenes on the imprinted Rh dimer is illustrated in Fig. 16.

The template ligand $P(OCH_3)_3$ possesses a similar shape to that of a half-hydrogenated species of 3-ethyl-2-pentene. To examine size and shape-selectivities by the molecular imprinting, eight alkenes including 3-ethyl-2-pentene were used as reactants for catalytic hydrogenation. Fig. 17 shows steady-state reaction rates (TOF) of the hydrogenation of eight alkenes at 348 K on the supported Rh-complex catalyst (Rh_{2sup}) and the molecular-imprinting catalyst (Rh_{2imp}). The homogeneous catalysts $Rh_2Cl_2(CO)_4$ and $RhCl(P(OCH_3)_3)_3$ and the attached $Rh_2Cl_2(CO)_4/SiO_2$ catalyst had no activities for the reaction. On the other hand, the Rh_{2sup} catalyst exhibited significant catalytic activities under the similar reaction conditions. It is to be noted that the hydrogenation reactions were remarkably promoted for all alkenes by the surface imprinting. The Rh_{2imp} catalyst was highly active as well as so durable that it could be used repeatedly in toluene solution. The catalytic hydrogenation proceeded linearly on the both catalysts and such linearities in the performance were observed for all alkenes employed in this study, indicating high durability of the catalyst. The active Rh_{2imp} catalyst was also air-stable, which is advantageous in practical handling of the system. The metal–metal bonding and coordinative unsaturation of the Rh dimer are key factors for the tremendous activity of the Rh_{2imp} catalyst.

The TOF for the alkene hydrogenation on the Rh catalysts remarkably depended on the nature of

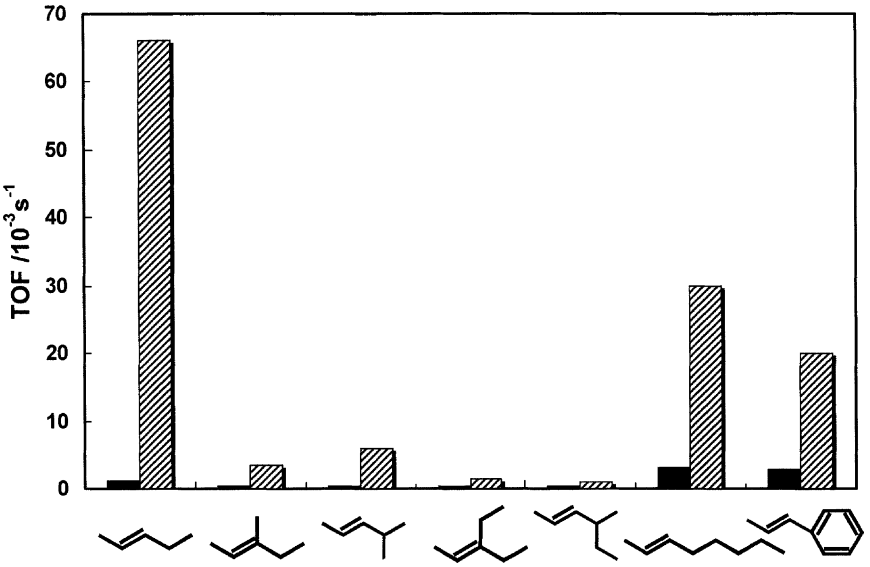

Fig. 17. Reaction rates for hydrogenation of seven alkenes on the supported (black) and imprinted (slash) Rh-dimer catalysts.

alkenes as shown in Fig. 17. Hydrogenation of linear alkenes like 2-pentene, 2-octene and 1-phenylpropene without any branch alkyl group near the C=C double bond were very fast on both Rh_{2sup} and Rh_{2imp} catalysts. On the other hand, branch alkenes such as 3-methyl-2-pentene, 4-methyl-2-pentene, 3-ethyl-2-pentene and 4-methyl-2-hexene were hard to hydrogenate compared with the linear alkenes. The reaction rates of 3-methyl-2-pentene and 3-ethyl-2-pentene with the methyl and ethyl branches at the C=C bond were slower than that of 4-methyl-2-pentene. Large ligands of metal complexes can regulate the reactivity of metal center electronically and geometrically to give higher selectivity than metal and metal oxide catalysts without any ligand. Surface-attached metal complexes are also subjected to regulation by the surface which is regarded as a unique and large ligand. Indeed, the Rh_{2sup} catalyst showed remarkable selectivities for the alkene hydrogenation as shown in Fig. 17. The hydrogenation rate of 2-pentene on the Rh_{2sup} catalyst was 19 times faster than those of 3-methyl-2-pentene and 4-methyl-2-pentene that have a methyl group at 3- and 4-carbon positions, respectively. In contrast to the branch alkenes, length of the alkene main chain did not affect negatively the reaction rate, for example, 2-pentene, 2-octene and 1-phenylpropene, as shown in Fig. 17.

Selectivity for the alkene hydrogenation on the Rh_{2imp} catalyst depends on the size and shape of the template cavity as reaction site in the micropores of the SiO_2-matrix overlayers on the Ox.50 surface in addition to the electronic and geometric effects of the ligands. To see the molecular-imprinting effect on the selectivity, we calculated the ratio of TOF of the Rh_{2imp} catalyst to TOF of the Rh_{2sup} catalyst for each alkene. The TOF ratios reduced with gain of alkene size as shown in Fig. 18. It is to be noted that there was a large difference between 3-ethyl-2-pentene and 4-methyl-2-hexene. Since a half-hydrogenated species of 3-ethyl-2-pentene is a similar shape to the template ligand $P(OCH_3)_3$, the big difference in the rate enhancement is due to the difference in the shape of the alkenes. The difference in the TOF ratios between 4-methyl-2-pentene and 4-methyl-2-hexene was so large, where the difference in the size of a methyl group is discriminated on the Rh_{2imp} catalyst. The TOF ratio for 4-methyl-2-hexene was much smaller than that for 2-pentene as shown in Fig. 18, where the difference in the alkenes is the size and shape by the ethyl group. There was also a big difference between 2-pentene and 2-octene, where a propyl group could be discriminated. Thus, the molecular-imprinting catalyst discriminates the size and shape of the alkenes. However, there was no significant difference in the TOF

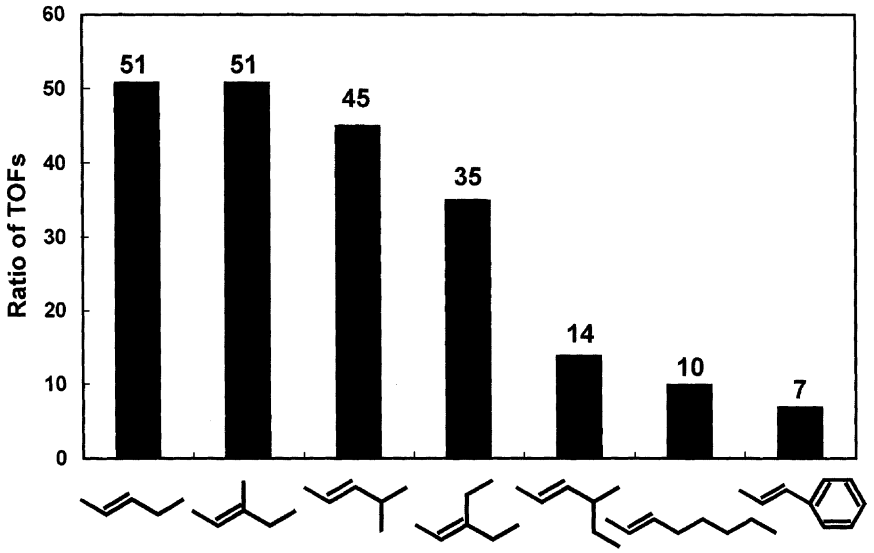

Fig. 18. Degrees of enhancement of the reaction rates at 348 K by molecular imprinting. Ratio of TOF is TOF of the imprinted catalyst to TOF of the supported catalyst.

ratios between 2-pentene and 4-methyl-2-pentene, between 3-methyl-2-pentene and 3-ethyl-2-pentene, and between 2-pentene and 3-ethyl-2-pentene as shown in Fig. 18. Thus, the molecular-imprinting catalyst could not discriminate the existence of methyl and ethyl groups among the smaller alkenes than the template size. It is noteworthy that the reaction rates of 2-pentene, 2-octene and 1-phenylpropene on the Rh_{2sup} catalyst were similar to each other, whereas the rate enhancements (TOF ratios) for 2-octene and 1-phenylpropene (10 and 7 times, respectively) were much less than that for 2-pentene (51 times). Because the length of linear alkene chains could not be discerned by ligand-coordinated metal site, it is suggested that the difference was caused by wall of the template cavity around the Rh-dimer site.

Activation energies for the hydrogenation on the Rh_{2sup} catalyst were divided into two values, about 30 and 42 kJ mol^{-1}, for the linear alkenes like 2-pentene, 2-octene and 1-phenylpropene, and the branch alkenes, respectively. Such a large difference in activation energy was also observed with Wilkinson complex. On the contrary, activation entropies for the hydrogenation on the Rh_{2sup} catalyst were similar to each other, which values were in the range -200 to -215 J mol^{-1} K^{-1} for all the alkenes.

After the imprinting, significant difference between small and large alkenes was observed in both activation energies and activation entropies. The activation energies for the hydrogenation of 3-ethyl-2-pentene and smaller alkenes than 3-ethyl-2-pentene (left four alkenes in Fig. 18) on the Rh_{2imp} catalyst were 26–43 kJ mol^{-1}, which were similar values to those observed on the Rh_{2sup} catalyst. The activation entropies for the four alkenes were -170 to -195 J mol^{-1} K^{-1}, which were larger than those (-200 to -210 J mol^{-1} K^{-1}) obtained for the Rh_{2sup} catalyst. In contrast, for the larger alkenes such as 4-methyl-2-hexene, 2-octene and 1-phenylpropene, the activation energies were 10, 7 and 8 kJ mol^{-1}, respectively, which were so small values compared with those for the Rh_{2sup} catalyst and other metal-complex catalysts. Furthermore, the activation entropies reduced prominently from about -210 to about -260 J mol^{-1} K^{-1}. The conspicuous change in the kinetic parameters for the larger alkenes was paralleled to the change in enhancement of the reaction rates. These dramatic reductions of the activation energy and the TOF ratio can be explained by shift of the rate-determining step from the alkyl formation to coordination of alkene to the Rh site as discussed in Section 4. Attended to this shift, the activation

entropies for those alkene molecules also decreased largely to about −260 from about −180 $J\,mol^{-1}\,K^{-1}$ for the other small molecules. It suggests that conformation of the coordinated alkene in the template cavity is regulated by wall of the cavity and remaining $P(OCH_3)_3$ ligands. For the alkenes with the larger sizes and different shapes compared to the template, the coordination to the Rh site through the cavity space becomes most slow in the reaction sequences.

6. Summary

In contrast to molecular imprinting of chromatographical adsorbents, gas sensing materials, etc. the design of molecular recognition and shape-selective metal-complex catalysts by molecular imprinting is still infancy. Achievement of more strict recognition of molecules needs further investigation. Nevertheless, the molecular imprinting at surfaces may be a promising way to design artificial enzymatic catalysts with 100% selectivity for target reactions. Further, the molecular-imprinting technique may also provide new catalytic systems with tremendous performances for reactions for which enzymes cannot be efficient at all and under the reaction conditions where enzyme systems cannot be applied. The combination of the attaching of metal-complex precursor on surface and molecular imprinting of the attached metal complex by amorphous inorganic and organic matrices may be an approach with wide applications to a variety of catalytic samples.

References

[1] P.A. Brady, J.K.M. Sanders, Chem. Soc. Rev. 26 (1997) 327.
[2] O. Ramstrom, R.J. Ansell, Chirality 10 (1998) 195.
[3] K.J. Shea, Trends Polym. Sci. 2 (1994) 166.
[4] K. Mosbach, Trends Biochem. Sci. (1994) 9.
[5] G. Wulff, in: W.T. Ford (Ed.), Polymeric Reagents and Catalysis, American Chemical Society, Washington, DC, 1986, p. 186.
[6] D.C. Sherrington, Chem. Commun. (1998) 2275.
[7] M.E. Davis, A. Katz, W.R. Ahmad, Chem. Mater. 8 (1996) 1820.
[8] M.J. Whitcombe, C. Alexander, E.N. Vulfson, Synlett 6 (2000) 911.
[9] B. Sellergren, Angew. Chem. Int. Ed. Engl. 39 (2000) 1031.
[10] K.J. Shea, D.Y. Sasaki, J. Am. Chem. Soc. 113 (1991) 4109.
[11] P.K. Dhal, F.H. Arnold, J. Am. Chem. Soc. 113 (1991) 7417.
[12] M.J. Whitcombe, M.E. Rodriguez, P. Villar, E.N. Vulfson, J. Am. Chem. Soc. 117 (1995) 7105.
[13] C. Yu, K. Mosbach, J. Org. Chem. 62 (1997) 4057.
[14] D. Spivak, K.J. Shea, J. Org. Chem. 64 (1999) 4627.
[15] J.U. Klein, M.J. Whitcombe, F. Mulholland, E.N. Vulfson, Angew. Chem. Int. Ed. Engl. 38 (1999) 2057.
[16] T. Takeuchi, A. Dobashi, K. Kimura, Anal. Chem. 72 (2000) 2418.
[17] B.R. Hart, D.J. Rush, K.J. Shea, J. Am. Chem. Soc. 122 (2000) 460.
[18] E. Yilmaz, K. Haupt, K. Mosbach, Angew. Chem. Int. Ed. Engl. 39 (2000) 2115.
[19] M.A. Khasawneh, P.T. Vallano, V.T. Remcho, J. Chromatogr. A 922 (1/2) (2001) 87.
[20] B. Sellergen, J. Chromatogr. A 906 (1/2) (2001) 227.
[21] K. Mosbach, Chem. Rev. 100 (2000) 2495.
[22] C. Malitesta, I. Losito, P.G. Zambonin, Anal. Chem. 71 (1999) 1366.
[23] E.P.C. Lai, A. Fafara, V.A. VanderNoot, M. Kono, B. Polsky, Can. J. Chem. 76 (1998) 265.
[24] L. Ye, K. Mosbach, J. Am. Chem. Soc. 123 (2001) 2901.
[25] M.W. Poljakow, J. Phys. Chem. 2 (1931) 799.
[26] F.H. Dickey, Proc. Natl. Acad. Sci. U.S.A. 35 (1949) 227.
[27] F.H. Dickey, J. Phys. Chem. 59 (1955) 659.
[28] K. Morihara, M. Kurosawa, Y. Kamata, T. Shimada, J. Chem. Soc., Chem. Commun. (1992) 358.
[29] K. Morihara, M. Takiguchi, T. Shimada, Bull. Chem. Soc. Jpn. 67 (1994) 1078.
[30] J.V. Beach, K.J. Shea, J. Am. Chem. Soc. 116 (1994) 379.
[31] G. Wulff, Angew. Chem. Int. Ed. Engl. 34 (1995) 1812.
[32] G. Wulff, T. Gross, R. Schonfeld, Angew. Chem. Int. Ed. Engl. 36 (1997) 1962.
[33] C. Alexander, C.R. Smith, M.J. Whitcombe, E.N. Vulfson, J. Am. Chem. Soc. 121 (1999) 6640.
[34] A.G. Strikovsky, D. Kasper, M. Grun, B.S. Green, J. Hradil, G. Wulff, J. Am. Chem. Soc. 122 (2000) 6295.
[35] B. Sellergren, R.N. Karmalkar, K.J. Shea, J. Org. Chem. 65 (2000) 4009.
[36] A. Katz, M.E. Davis, Nature 403 (2000) 286.
[37] K. Morihara, S. Kurihara, J. Suzuki, Bull. Chem. Soc. Jpn. 61 (1988) 3991.
[38] D.K. Robinson, K. Mosbach, J. Chem. Soc., Chem. Commun. (1989) 969.
[39] J. Heilmann, W.F. Maier, Angew. Chem. Int. Ed. Engl. 33 (1994) 471.
[40] M.A. Markowitz, P.R. Kust, G. Deng, P.E. Schoen, J.S. Dordick, D.S. Clark, B.P. Gaber, Langmuir 16 (2000) 1759.
[41] T. Tanimura, N. Katada, M. Niwa, Langmuir 16 (2000) 3858.
[42] A. Suzuki, M. Tada, T. Sasaki, T. Shido, Y. Iwasawa, J. Mol. Catal. A: Chem. 182/183 (2002) 125.
[43] J. Matsui, I.A. Nicholls, I. Karube, K. Mosbach, J. Org. Chem. 61 (1996) 5414.
[44] F. Locatelli, P. Gamez, M. Lemaire, J. Mol. Catal. A: Chem. 135 (1998) 89.
[45] B.P. Santora, A.O. Larsen, M.R. Gagne, Organometallics 17 (1998) 3138.

[46] K. Polborn, K. Severin, Chem. Eur. J. 6 (2000) 4604.
[47] K. Polborn, K. Severin, Eur. J. Inorg. Chem. (2000) 1687.
[48] A.N. Cammidge, N.J. Baines, R.K. Bellingham, Chem. Commun. (2001) 2588.
[49] M. Tada, T. Sasaki, Y. Iwasawa, Phys. Chem. Chem. Phys. 4 (2002) 4561.
[50] M. Tada, T. Sasaki, Y. Iwasawa, J. Catal. 211 (2002) 496.
[51] M. Tada, T. Sasaki, T. Shido, Y. Iwasawa, Phys. Chem. Chem. Phys. 4 (2002) 5899.
[52] Y. Fujii, K. Matsutani, K. Kikuchi, J. Chem. Soc., Chem. Commun. (1985) 415.
[53] J. Suh, Y. Cho, K.J. Lee, J. Am. Chem. Soc. 113 (1991) 4198.
[54] J.F. Krebs, A.S. Borovik, J. Am. Chem. Soc. 117 (1995) 10593.
[55] J.F. Krebs, A.S. Borovik, Chem. Commun. (1998) 553.
[56] N.M. Brunkan, M.R. Gagne, J. Am. Chem. Soc. 122 (2000) 6217.
[57] Y. Iwasawa, Adv. Catal. 35 (1987) 187.
[58] Y. Izumi, H. Chihara, H. Yamazaki, Y. Iwasawa, J. Phys. Chem. 98 (1994) 594.
[59] K. Asakura, K.K. Bando, Y. Iwasawa, H. Arakawa, K. Isobe, J. Am. Chem. Soc. 112 (1990) 9096.
[60] K.K. Bando, K. Asakura, H. Arakawa, K. Isobe, Y. Iwasawa, J. Phys. Chem. 100 (1996) 13636.
[61] Y. Iwasawa, in: Proceedings of the 11th International Congress on Catalysts, Baltimore, Stud. Surf. Sci. Catal. 101 (1996) 21.
[62] Y. Iwasawa, Acc. Chem. Res. 30 (1997) 103.